ADVANCED ENERGY MATERIALS
www.advenergymat.de

Parasitic Absorption and Internal Quantum Efficiency Measurements of Solid-State Dye Sensitized Solar Cells

*George Y. Margulis, Brian E. Hardin, I-Kang Ding, Eric T. Hoke, and Michael D. McGehee**

The internal quantum efficiency (IQE) of solid-state dye sensitized solar cells (ssDSCs) is measured using a hybrid optical modeling plus absorptance measurement approach which takes into account the parasitic absorption of the hole transport material (HTM). Across device thicknesses of 1 to 4 microns, ssDSCs sensitized with Z907 and TT1 dyes display relatively constant IQEs of approximately 88% and 36%, respectively, suggesting excellent charge collection efficiencies for both dyes but poor carrier injection for TT1 devices. The addition of more coadsorbent is shown to increase the IQE of TT1 up to approximately 58%, but significantly lowers dye loading. Finally, optical losses due to absorption by the HTM are quantified and found to be a significant contribution to photocurrent losses for ssDSCs sensitized with poor absorbers such as Z907, as the weak absorption of the dye gives the HTM opportunity for significant parasitic absorption within the active layer.

1. Introduction

Recently, there has been a flurry of research interest in solid-state dye sensitized solar cells (ssDSCs), a promising solar technology which makes use of low-cost, abundant materials and relatively simple processing conditions.[1–7] While dye sensitized solar cells based on a liquid electrolyte have reached efficiencies in excess of 12%,[8,9] current ssDSC record efficiencies stand near 7%.[10,11] An important quantity in understanding the performance of solar cells is the external quantum efficiency (EQE), defined as the ratio of charge carriers collected divided by number of incident photons (as a function of wavelength). The EQE of liquid dye sensitized solar cells (DSCs) is typically 85% at peak absorption, as approximately 15% of incident photons are reflected or absorbed within the F:SnO_2 (FTO) electrode, and the remainder are absorbed in the 10-μm-thick cells and then converted to collected charge with an efficiency of near 100%.[12] In contrast, the peak EQE of ssDSCs is frequently only 30% to 75%.[11,13] Because ssDSC devices optimize at a thickness of approximately 2 μm, this lower EQE can stem from incomplete light harvesting, competitive absorption by non-photoactive layers or electronic losses, such as charge recombination or inefficient charge injection.[14,15] It is important to disentangle these absorption losses in the various layers of the ssDSC with electronic losses for a full understanding of device operation.

Internal quantum efficiency (IQE) is a useful device metric which measures a solar cell's ability to convert photons absorbed within the active material into electrons, and allows for diagnosis of charge collection and absorption problems.[12] In ssDSCs, the notion of IQE may be a bit ambiguous, as the active layer consists of a mesoporous network of TiO_2 nanoparticles, an adsorbed sensitizing dye, and infiltrated HTM (typically 2,2′,7,7′-tetrakis-(*N*,*N*-di-*p*-methoxyphenylamine)9,9′-spirobifluorene, known as spiro-OMeTAD). However, since absorbed light by spiro-OMeTAD does not lead to photocurrent (additional discussion in the supporting information), a natural definition for IQE in ssDSCs would be electrons collected in the device divided by photons absorbed by the sensitizing dye within the active layer. Although UV photons absorbed by titania can generate a modest amount of photocurrent, because the titania does not significantly absorb in the visible, this definition of IQE quantifies the ability of the dye to convert visible light into collected charge carriers. IQE is an important parameter that is used in diagnosing current losses, current matching tandem devices, and characterization of liquid DSCs and organic solar cells.[16–18]

Calculation of the IQE requires both measurement of the EQE and knowledge of the percentage of light (i.e., absorptance) that is absorbed by the photoactive material. In liquid DSCs, the dye and titania absorptance can be relatively accurately measured by comparing the transmission through a sensitized titania DSC electrode with the transmission through an unsensitized substrate. While this method neglects some reflection and scattering effects, such errors tend to be

G. Y. Margulis
Department of Applied Physics
Stanford University
Geballe Laboratory for Advanced Materials
476 Lomita Mall, Stanford, CA, 94305, USA
Dr. I.-K. Ding, Dr. E. T. Hoke, Prof. M. D. McGehee
Department of Materials Science and Engineering
Stanford University
Geballe Laboratory for Advanced Materials
476 Lomita Mall, Stanford, CA, 94305, USA
E-mail: mmcgehee@stanford.edu
Dr. B. E. Hardin
Molecular Foundry
Lawrence Berkeley National Laboratory
67 Cyclotron Road, Berkeley, California, 94720, USA

DOI: 10.1002/aenm.201300057

© 2013 WILEY-VCH Verlag GmbH & Co. KGaA, Weinheim

relatively negligible in typical DSCs with 10-μm-thick, strongly absorbing active layers. In contrast, ssDSCs utilize a silver back contact which does not allow for such a simple measurement of the photoactive layer absorptance. Thus, optical modeling based on measured indices of refraction has been used to calculate the absorptance of the photoactive layer for IQE measurements.[19,20] However, accurate optical modeling of ssDSCs is difficult due to the large number of layers, uncertainty in the indices of refraction, interference effects and scattering. Large errors in optical modeling (20% or more) are propagated and result in similarly large errors in internal quantum efficiency. It should also be noted that these same problems exist for IQE measurements of other devices with similar structures, such as ssDSC analogs with inorganic absorbers or meso-superstructured solar cells (MSSCs).[21–25]

In this work, we use a combination of measurements and optical modeling calculations to accurately determine what fraction of incident light is absorbed by the dye and what fraction is absorbed parasitically by materials that do not generate photocurrent, such as FTO and the HTM. This information allows for accurate measurements of the IQE, from which we elucidate valuable information about electronic losses within the device. The internal quantum efficiency of two common sensitizing dyes was investigated: Z907, a broadly absorbing Ru-based dye, and TT1, a Zinc-phthalocyanine-based red-absorbing sensitizer.[26,27] Both Z907 and TT1 have shown high performance in liquid electrolyte DSCs, but TT1 shows relatively poor performance in ssDSCs, with efficiencies around 1%. Z907, on the other hand, was selected as it has been widely studied as a sensitizer in ssDSCs and achieves efficiencies of approximately 4%.[27] Additionally, both TT1-based and Z907-based devices show excellent reproducibility.

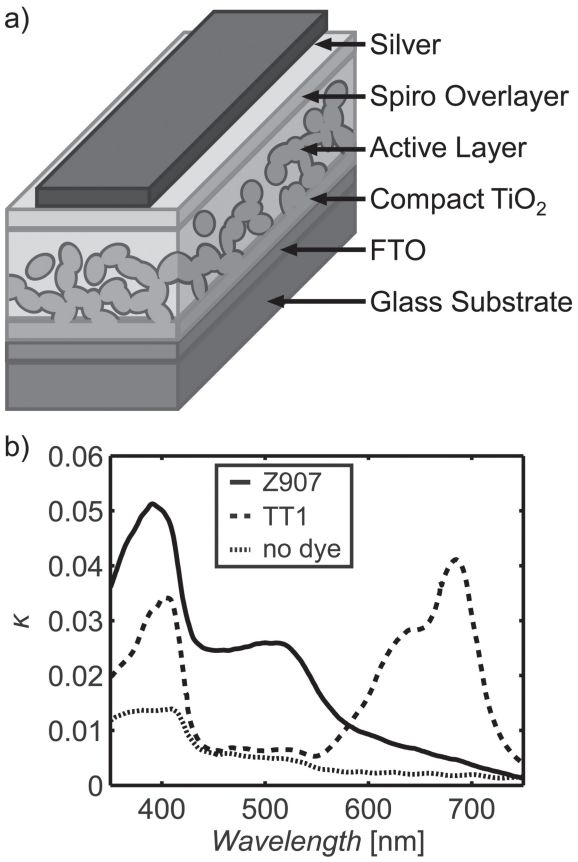

Figure 1. (a) Schematic diagram of ssDSC layers. (b) Imaginary portion of index of refraction of Z907-dyed active layer, TT1-dyed active layer, and undyed active layer as measured by optical absorption. The imaginary component of the index of refraction, κ, is related to the thin film absorption coefficient, α, by $\alpha = 4\ \pi\kappa/\lambda$, where λ is the wavelength of light.

2. Measurement of IQE

A ssDSC can be viewed as a stack of 6 layers: a glass substrate, F:SnO_2 (FTO) layer, TiO_2 compact layer, an active layer, spiro-OMeTAD overlayer, and silver electrode (device architecture shown in **Figure 1**a. In addition to the parasitic absorption in the glass, FTO, compact TiO_2, spiro-OMeTAD overlayer and silver back contact, there is additional parasitic absorption within the active layer by infiltrated spiro-OMeTAD and titania. When light is incident on the ssDSC, a fraction is absorbed by the dye, with the rest being reflected or lost by absorption within these non-photoactive materials (termed the parasitic absorptance). In order to accurately measure the fraction of light absorbed by the dye, a hybrid modeling-experimental approach was used that has previously been applied to thin film organic solar cells.[18] This technique relies primarily on measurements of the device absorptance, using optical modeling as only a small correction. This approach is particularly well-suited to ssDSCs due to the difficultly of performing accurate optical simulations of ssDSCs. First, the reflectance of the entire ssDSC device, R_{device}, is measured using an integrating sphere to account for diffuse reflection due to scattering. Since the silver back contact allows no transmission, the measured absorptance of the device is given by $ABS_{measured,DSC}$ = (1-R_{device}). The absorptance of each layer of the solid-state dye sensitized solar cell is then modeled using methods discussed in subsequent sections, and the modeled parasitic absorptance is summed to give $ABS_{modeled,parasitic}$. While in our experience, typical optical modeling can have an error of 20% or more, primarily due to errors in index of refraction values, $ABS_{modeled,parasitic}$ is generally only 25% or less of $ABS_{measured,DSC}$, leading to only a small error in the total measurement of photons absorbed by the dye, which is given by $ABS_{measured,DSC} - ABS_{modeled,parasitic}$ (for example, 20%×25% error = 5% error). The IQE can then be calculated as

$$IQE = \frac{EQE}{\left(ABS_{measured,DSC} - ABS_{modeled,parasitic}\right)} \quad (1)$$

Optical modeling uses the optical properties of materials to calculate the reflection and absorption of incident light within the ssDSC device stack. A convenient method of modeling layered materials is the transfer matrix approach, which has been previously applied to ssDSCs and organic solar cells, and has calculation code readily available online.[18,19,28] The inputs for transfer matrix modeling (and many optical modeling methods) are the complex indices of refraction (as a function of wavelength) and thicknesses of each layer in the

© 2013 WILEY-VCH Verlag GmbH & Co. KGaA, Weinheim

device. Layer thicknesses can be measured through cross-sectional SEM microscopy (sample image shown in Supporting Information Figure S3). Indices of refraction of thin films are typically measured through variable angle spectroscopic ellipsometry (VASE), and indices of refraction for all ssDSC layers are contained in literature.[20] The index of refraction can be written as a real portion, n, and a complex portion, κ, with κ related to the thin film absorption coefficient, α, by $4\pi\kappa/\lambda$. While VASE is a difficult measurement that requires complex fitting, the absorption coefficient, α, and therefore κ, can also be measured for strongly absorbing layers by simple absorption measurements. By measuring absorptance of a thin film of a given thickness,x, the absorption coefficient, α, can be calculated using Beer's Law: the intensity of transmitted light, I, is given by $I = I_0e^{-}\alpha x$, where I_0 is the incident light intensity. In order to get more accurate values of κ, it is ideal to average the absorption coefficient over multiple thin film thicknesses to minimize measurement errors as well as errors due to optical interference from reflections. While this measurement neglects reflections and scattering, these effects are typically small (<10%) for thin films of the various layers in ssDSCs. It was found that these measured complex index of refraction values lead to much better correlation between the modeled and measured absorptance of dye-sensitized films and devices than κ values from VASE. Errors in the real portions of the indices of refraction, n, can also cause modeling errors, as they determine reflections at the interfaces between layers. For ssDSCs, the mismatches between n at layer interfaces tend to be relatively small, leading to small reflections (with the exception being reflection off the silver back contact). Hence, any inaccuracy in the value of n tends to cause less total error in calculating IQE than inaccuracy in the measurement of κ. In fact, the same spectrum for n can be used for modeling the active layer independent of which sensitizing dye was used, resulting in a negligible error. For our modeling, the indices of refraction were taken from literature, except for the active mesoporous layer, FTO, and glass, when the strong absorption of the ssDSC layer allowed for a direct measurement of the absorption coefficient.[20]

As mentioned previously, the mesoporous active layer contains 3 principal components: dye, titania and HTM, and it is important to decouple the parasitic absorption of the HTM from the absorptance of the dye. The index of refraction of the active layer can be written as $n_{active} + i\kappa_{active}$, where the κ_{active} can be split into the sum of κ_{dye} and $\kappa_{parasitic}$. κ_{active} can be measured from the absorption of the dye-sensitized active layer, while $\kappa_{parasitic}$ can be measured from the absorption of an unsensitized active layer. Given the total absorptance of the active layer, ABS_{active}, the parasitic absorptance within the active layer can then be calculated as $ABS_{modeled,active\ parasitic} = (\kappa_{parasitic}/\kappa_{active})ABS_{active}$. Measured κ values of the active layer with no sensitizer and with both the TT1 and Z907 dyes are depicted in Figure 1b; while the dye, titania and spiro-OMeTAD all absorb very strongly below 425 nm, the absorption above 425 nm is dominated by the dye and a small but significant contribution by oxidized spiro-OMeTAD.[29–31] Simply looking at the relative magnitudes of the imaginary portion of the index of refraction suggests that the parasitic absorption within the active layer causes significant losses.

Given the indices of refraction and layer thicknesses for each layer in the ssDSC, transfer matrix modeling is used to calculate the absorptance for each layer. In layered thin film devices reflections off the interfaces between layers can cause constructive or destructive interference, resulting in an absorptance that 'oscillates' as a function of wavelength. Optical modeling using the transfer matrix method assumes each layer is of uniform thickness, which leads to very strong optical interference fringes (See Figure S1 in the Supporting Information). In reality the thickness of the ssDSC layers (particularly the active layer) varies throughout the device, which partially averages out the interference fringes expected by transfer matrix modeling. To account for this thickness variation, the absorptance resulting from transfer matrix modeling was averaged by changing the active layer by ±5% of the measured thickness. Modeled absorptance of each component of a Z907-sensitized ssDSC is shown in **Figure 2**a and the total modeled device absorptance is compared to measured ssDSC absorptance in Figure 2b. As can be seen, our modeling approach (utilizing averaging) resulted in a smoother absorptance that matched experiment relatively well.

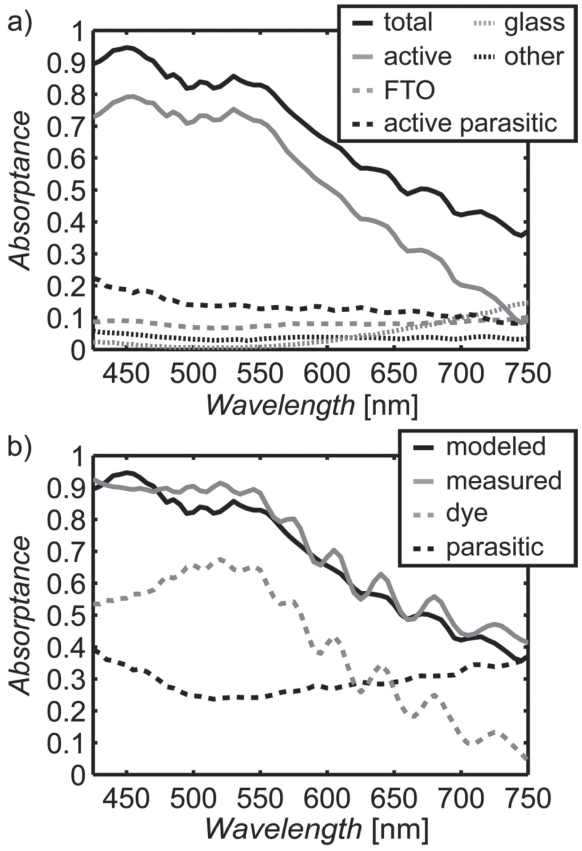

Figure 2. (a) Modeled absorptance for each layer of a 2.3-µm-thick Z907 ssDSC: total device absorptance, active layer absorptance, FTO absorptance, parasitic absorptance within the active layer, glass absorptance, and sum of the absorptances of other layers (TiO_2 compact layer, spiro-OMeTAD overlayer and silver cathode). (b) Comparison of modeled and measured device absorptance. Total modeled parasitic absorptance is shown as a dashed black line and the dye absorptance, $ABS_{measured,DSC}$-$ABS_{modeled,parasitic}$, is depicted by the dashed gray line.

© 2013 WILEY-VCH Verlag GmbH & Co. KGaA, Weinheim

In principle, a variety of optical simulation techniques actually result in similar IQE values if accurate optical parameters are used in conjunction with the hybrid measurement/modeling approach. Hence specific details of our optical modeling are contained in the Supporting Information along with discussion comparing ssDSC absorptances and IQEs calculated using different model assumptions. This exemplifies the strength of this hybrid approach to measuring IQE: errors in modeling do not substantially affect the calculated IQE as the majority of the photoactive layer absorptance comes from directly measuring the reflectance of the ssDSC device.

3. Results and Analysis

3.1. IQE for Z907 and TT1 ssDSCs

Once the absorptance of all the parasitic layers is calculated, it is straightforward to apply Equation 1 to calculate the IQE. The dye absorptance, EQE and calculated IQE for a Z907 ssDSC and a TT1 ssDSC are shown in **Figure 3**. Due to uncertainty in the material optical parameters and layer thicknesses, the interference fringes in the calculated absorptance and measured EQE do not occur at the same wavelengths. Consequently, the calculated IQE has a small oscillating component, particularly for Z907 devices, as depicted in Figure 3a. In principle, the IQE of a ssDSC should be constant with respect to wavelength, and if the modeling was perfect, the absorptance of the dye should be proportional to the EQE times a constant value. Using this hybrid approach allows for minimizing any errors such as interference peak mismatches between the modeling and measurement to achieve as flat an IQE as possible. In order to get a good measure of the exact IQE of each device, the calculated IQE was averaged in the wavelength regime where the dye absorption was highest (440–560 nm for Z907 dye and 620–705 nm for TT1 dye). Because the dye absorbs the majority of the photons in this regime, these are the wavelengths for which the IQE is most accurate. To quantify the error in the measurement, the modeled parasitic absorptance was changed by ±20% and the resulting IQE is shown by the dotted lines (Figure 3). In the regime where the dye absorbs strongly, errors in modeling lead to errors of 10% or less in IQE. As shown in Figure 3b, for TT1-based ssDSCs, the IQE is almost completely flat in the red portion of the spectrum where the dye absorption is strongest.

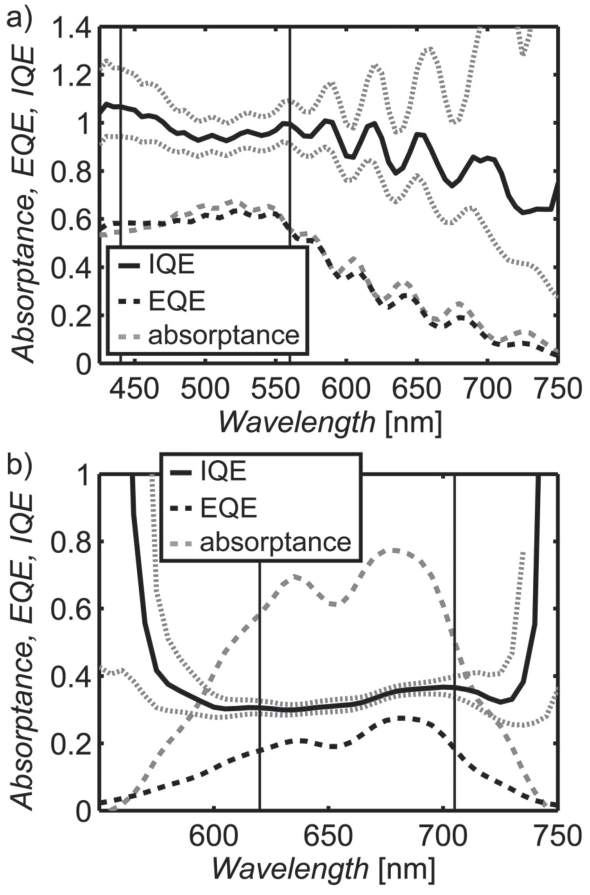

Figure 3. Dye absorptance as given by $ABS_{measured,DSC}$-$ABS_{modeled,parasitic}$, measured EQE, and calculated IQE plots for (a) 2.3-µm-thick Z907 device and (b) 2.2-µm-thick TT1 device. Dotted gray lines denote error bars in IQE measurement based on a ±20% error in modeling parasitic absorptance. Vertical black lines depict averaging range for calculating a single IQE value for each device.

Figure 4 shows the IQE of Z907 and TT1 ssDSCs for active layer thicknesses between 1 and 4 microns. In this thickness range, the pore-filling fraction remains high enough to not limit performance, and due to the large diffusion length at short-circuit (significantly longer than the film thickness), the IQE of both the Z907 and TT1 devices stays constant.[32–34] The constant IQE with thickness suggests that charge collection is not a problem in these devices even at thicknesses that are larger than the ideal thickness of approximately 2 microns. The losses in efficiency, rather, come from the decreasing voltage

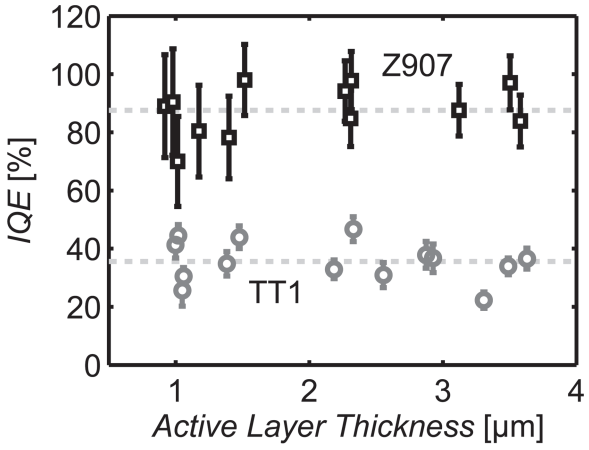

Figure 4. IQE vs. active layer thickness for Z907 (black squares) and TT1 (gray circles) ssDSCs. Error bars are calculated from the standard deviation of the IQE in the measurement range summed in quadrature with the average error in IQE caused by increasing/decreasing the parasitic absorption by 20% (depicted by gray dotted lines in Figure 3). This error metric takes into account uncertainty caused by large amounts of parasitic absorption and not-flat IQEs caused by inaccuracies in modeling and/or measurement. Error bars are larger for thinner devices due to the relatively low dye absorptance in the ssDSC. The light gray dashed lines depict the average IQE for Z907 and TT1 devices.

© 2013 WILEY-VCH Verlag GmbH & Co. KGaA, Weinheim

with thickness and decrease in fill factor.[35] However, while the IQE of Z907 stays high at 88%, the average IQE of the TT1 cells is only approximately 36%, suggesting there is a significant electron or hole injection problem with the TT1 dye into the TiO_2 or spiro-OMeTAD, respectively, leading to a near 60% loss. While TT1 has near 100% IQE in liquid DSCs, it displays significantly lower IQE in solid-state devices. The electron injection efficiency of TT1 in liquid DSCs is near unity, but it should be noted that the TiO_2 conduction band energy levels can be very different in solid-state and liquid devices due to the presence of additives such as *tert*-butylpyridine and Li^+, which can lead to different electron injection efficiencies.[36] It has been seen that the lowest unoccupied molecular orbital, or LUMO, of phthalocyanine dyes is lower than that of N719 (a dye similar to Z907), which can cause to poor electron injection efficiencies in liquid DSCs under certain electrolyte compositions.[37] Thus, it is hypothesized that the TiO_2 conduction band in solid-state devices is at an energy level which allows for efficient electron injection from the Z907 dye to the titania, but is too high for efficient TT1 electron injection. However, there are additional factors such as dye aggregation which can affect dye electron and hole injection efficiencies.

3.2. Effect of Coadsorbent on IQE

Many phthalocyanine dyes such as TT1 exhibit a tendency to aggregate due to π–π interactions between macrocycles.[38] A variety of strategies have been used to suppress aggregation, such as the addition of bulky substituents and the addition of coadsorbents.[38,39] It has been reported that the addition of coadsorbents such as chenodeoxycholic acid (cheno) can improve the efficiency of liquid DSCs through a variety of ways, including increasing charge injection efficiency by decreasing aggregation.[38,40,41] Coadsorbents, however, displace dye molecules on the titania surface and consequently decrease dye loading. While the reduction in dye loading does not severely decrease light absorption in 10-µm-thick liquid cells, it is problematic in thinner ssDSCs, where there is a need to maximize dye coverage within the limited thickness of the mesoporous titania layer. Coadsorbents have been investigated in ssDSCs as a means of improving efficiency,[42–44] but the effect of coadsorbents on IQE has not been investigated.

To investigate the effect of the suppression of aggregation on TT1 ssDSCs, the cheno concentration was raised from 10 mM to 60 mM during dye sensitization, which has been shown to significantly decrease aggregation.[38] The additional cheno adsorption results in significantly lowered dye loading and absorption, necessitating the use of device active layers between 3.5–4 µm to ensure adequate dye absorption for accurate IQE quantification. Device optical modeling and absorptance is shown in **Figure 5**. Despite the low absorption of the active layer, the absorptance of the device at the dye's peak wavelength of 690 nm is still 0.74. However, from the optical modeling, it can be seen that nearly half of this absorptance can be attributed to the parasitic layers within the device. As shown in Figure 5, the high cheno TT1 ssDSCs display an average IQE of 58%. Since cheno has been shown to raise the conduction band of TiO_2 (i.e. lower electron affinity),[45] the increased internal quantum efficiency is attributed to an improved injection efficiency caused by suppression of dye aggregation rather than a shift in the TiO_2 conduction band. While an increase of 20% in IQE is significant, and deaggregation is an important consideration for the improvement of dye performance in ssDSCs, the IQE remains well below 100%, indicating that there are additional loss mechanisms such insufficient driving force for charge injection from the excited dye into the TiO_2 conduction band.

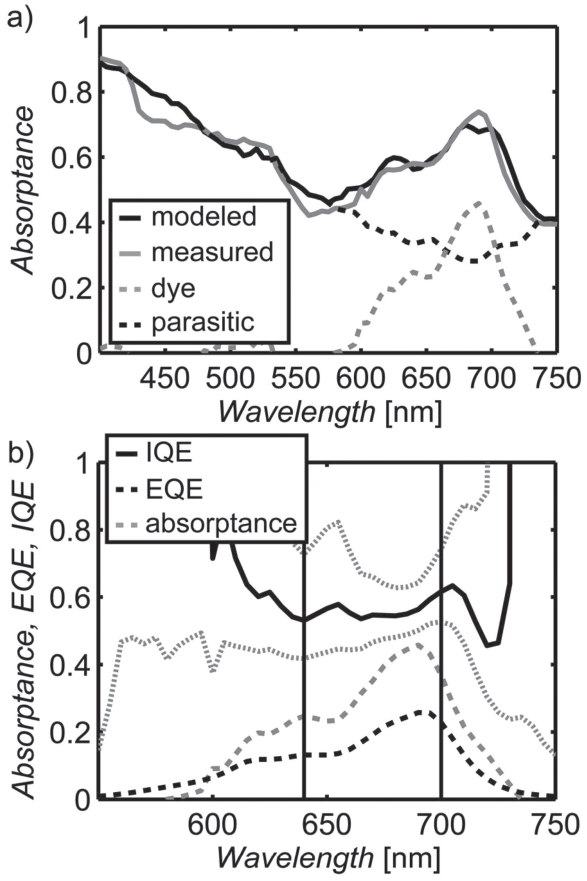

Figure 5. a) Comparison of modeled and measured absorptance for a high cheno (60 mM) TT1-sensitized device with an active layer thickness of 3.7 µm. Total modeled parasitic absorptance is shown as a dashed black line and $ABS_{measured,DSC}$-$ABS_{modeled,parasitic}$ is depicted by the dashed gray line. The solid and dashed black lines overlap where all the absorptance is due to non-photoactive materials (400–575 nm). b) IQE, EQE and $ABS_{measured,DSC}$-$ABS_{modeled,parasitic}$ for same device. Dotted gray lines denote error bars in IQE measurement based on a ±20% error in modeling parasitic absorptance. Vertical black lines depict the averaging range used for calculating a single IQE value.

3.3. Quantification of Parasitic Absorption Losses

Finally, the high IQE of Z907 also warrants discussion, as the peak EQE of the same devices remains at 60% or less, even for thicker films. Compared to many D-π-A dyes being developed for solid-state dye sensitized solar cells, Z907 is a relatively weak absorber. However, both modeling and measurements

© 2013 WILEY-VCH Verlag GmbH & Co. KGaA, Weinheim

suggest that the cell is able to absorb nearly all of the light (85–90%) at the dye's absorption peak in optimized 2-μm-thick devices. The low EQE is caused by the significant parasitic absorption of spiro-OMeTAD in the 450–550 nm wavelength range, which can be attributed to the oxidized form of spiro-OMeTAD.[29] While undoped spiro-OMeTAD does not appreciably absorb visible light, oxidized spiro-OMeTAD is necessary to achieve sufficient conductivity to make efficient devices and minimize series resistance losses.[10,29] Although more strongly absorbing dyes are able to outcompete spiro-OMeTAD for light absorption in this wavelength regime, Z907-based ssDSCs lose a very significant amount of light to the parasitic absorption in the active layer itself. These losses in photocurrent due to parasitic absorption within the active layer were quantified through optical modeling in order to understand the potential for increasing device efficiency. Because Z907 is such a weak absorber, if the parasitic absorption within the active layer were reduced to zero, there would be a nearly 14% gain in photocurrent, increasing the short-circuit current (J_{SC}) from 7.32 to 8.49 mA/cm^2. Thus, non-photoactive material within the active layer accounts for the largest source of parasitic absorption loss in Z907-sensitized ssDSCs. However, if the dye absorption in the Z907 active layer were 10 times larger, the loss due to parasitic absorption would only be approximately 2.8%, making this active layer absorption a reasonable target (corresponding to an absorption coefficient of 5–6 μm^{-1}) for ensuring losses due absorption by oxidized spiro-OMeTAD are small. A summary of the losses due to parasitic absorption is given in the Supporting Information (Table S1).

These results explain why increasing the thickness of Z907 devices does not bring the EQE above 60%: despite the short-circuit charge collection efficiency remaining constant, there is very little unabsorbed photon flux. Thus, techniques to increase light harvesting such as light trapping[46] or increasing device thickness would have only a minimal effect for wavelengths below 550 nm. Furthermore, any additional absorption would be split between the parasitic absorption of spiro-OMeTAD in the active layer and the dye, leading to even less additional photocurrent. On the other hand, D-π-A dyes have seen great success in ssDSCs with peak EQE's approaching 80%, which can be understood through the high absorption coefficient allowing the dye to outcompete spiro-OMeTAD for absorption below 550 nm.[11,13] Spiro-OMeTAD has also been used as the hole transport material in MSSCs utilizing an inorganic perovskite absorbing layer.[21–23] The absorption coefficient reported for such devices appears to be 5–10 times stronger than that of Z907-based ssDSCs and significantly reduces parasitic absorption in the active layer.

4. Conclusion

While internal quantum efficiency is a particularly useful metric for the analysis of photovoltaics, the difficulty in either modeling or measuring the absorptance of the dye in a ssDSC device has made IQE a difficult quantity to accurately calculate for ssDSCs. Hence, a hybrid approach utilizing optical modeling and absorption measurements is necessary for an accurate quantification of the internal quantum efficiency of ssDSCs due to the multitude of materials and layers in the device. This approach has been used to measure the IQE of ssDSCs using 2 sensitizers: TT1 and Z907, and elucidate interesting facts about their photovoltaic performances. The IQE of Z907-based ssDSCs is calculated to be approximately 90%, suggesting that nearly all charge carriers generated in by the sensitizing dye itself make it to the electrodes at short-circuit. On the other hand, TT1-based ssDSCs display significantly lower IQEs due to low charge injection efficiency, despite having near unity IQE in typical liquid electrolyte devices. Coadsorbents such as chenodeoxycholic acid can be used to increase injection efficiency by decreasing aggregation, but at the cost of dye absorptance due to competition for adsorption onto the mesoporous titania. Finally, the parasitic absorption in the active layer was found to be the largest optical loss in Z907-sensitized solar cells. Increasing the absorption within the active layer is an important goal for increasing the efficiency of solid-state dye sensitized solar cells, which are to be limited to 2 microns due to charge transport. However, increasing device thickness and light trapping also lead to increased spiro-OMeTAD absorption and significant optical losses. Even though the best performing dyes are able to convert photons to electrons at near-unity yields, research into new less absorbing hole transport materials and strongly absorbing dyes will be required to mitigate parasitic absorption losses and help push ssDSCs to new record efficiencies. Accurate internal quantum efficiency measurements are an important diagnostic tool in helping understand the various loss mechanisms in ssDSCs and continuing progress in the field.

5. Experimental Section

Device Fabrication: TiO_2 substrates were fabricated and sensitized with dye as previously reported.[34] FTO substrates (TEC15, Hartford Glass Co.) were cleaned by sequentially sonicating in detergent, acetone and isopropanol, with subsequent UV-ozone treatment for 20 minutes. Approximately 50–100 nm of compact TiO_2 was deposited using spray pyrolysis of titanium diisopropoxide bis(acetylacetonate) (Aldrich 75 weight% in isopropanol, diluted 10x with isopropanol). Films of varying titania thickness were doctorbladed by using transparent 18 nm TiO_2 nanoparticle paste (Dyesol, NR-18T) diluted with terpinoel resulting in nanoparticle films of thicknesses between 1 and 4 μm. Films were then sintered at 500 °C for 30 minutes. Subsequently, titania films were immersed in $TiCl_4$ solution overnight and sintered once again at 500 °C for 30 minutes. Titania substrates were then sensitized by immersion for 18 hours in a 0.3 mM solution of Z907 dye (Solaronix) in a 50:50 *tert*-butanol:acetonitrile or immersion for 4 hours in a 0.1 mM solution of TT1 dye in ethanol with 10 mM chenodeoxycholic acid.

Spiro-OMeTAD solution contained spiro-OMeTAD (Luminescence Technology corporation), *tert*-butylpyridine (4-tbp) and Lithium bis(trifluoromethylsulfonyl)imide salt (Li-TFSI) (pre-solved in acetonitrile). Li-TSFI solution was first made by dissolving 170 mg/ml Li-TSFI in acetonitrile. Spiro-OMeTAD solution was made by taking a 1 g spiro-OMeTAD: 97 mL 4-tbp: 208 mL Li-TSFI solution mixture dissolved in chlorobenzene (approximately 100–400 mg spiro-OMeTAD/mL chlorobenzene). The concentration of spiro-OMeTAD was varied to ensure adequate pore filling - which depends on the thickness of the TiO_2 nanoparticle film. The spiro-OMeTAD solution was then infiltrated by spincoating as previously reported, with spiro-OMeTAD concentration chosen to ensure a small (approximately 200 nm) but visible overlayer and maximal pore-filling.[33,34] Finally, a 200 nm silver cathode was deposited by thermal evaporation at a pressure of approximately

© 2013 WILEY-VCH Verlag GmbH & Co. KGaA, Weinheim

10^{-6} torr. All films and devices were subject to 15 minutes light soaking before measurement. Films used for measuring κ values were made on plain glass substrates with the film deposited with the same method as in actual ssDSC device fabrication.

EQE and Absorption Measurements: External quantum efficiency measurements were performed at a chopping rate of 40 Hz with a white light illumination bias of approximately 0.1 suns applied using an incandescent bulb powered by a DC voltage source. For the chopped EQE beam, a Newport Apex monochromator illuminator was used in conjunction with a Princeton Instruments monochromator and a filter wheel. The signal from the ssDSC was put through a transimpedance amplifier and recorded on a Stanford Instruments lock-in amplifier. The EQE Calibration was performed using a calibrated photodiode of known EQE. The EQE beam was split with a 50:50 beam splitter into a 2nd 'reference' photodiode that was used to correct for any fluctuations in the EQE beam source intensity.

Experimental set-up for absorptance measurements has also been reported.[18] Device absorptance measurements were performed using the same light source/monochromator as the EQE and measured using an integrating sphere with an attached silicon photodiode. Care must be taken to ensure that the incidence angle of the light should be as close to normal as possible, otherwise absorption and EQE measurements can display misaligned interference effects.

Layer Thickness measurements: Device layer thicknesses were measured with cross-sectional scanning electron microscopy using a FEI XL30 Sirion SEM and image processing software (ImageJ).[18]

Supporting Information

Supporting Information is available from the Wiley Online Library or from the author.

Acknowledgements

This work was supported by the Office of Naval Research (ONR) under grant N000141110244. We thank Professor Tomas Torres (Universidad Autónoma de Madrid) for providing TT1 dye. G.Y.M. would like to acknowledge the support of the ABB Stanford Graduate Fellowship in Science and Engineering. We also would like to thank Eva Unger for help in editing the manuscript.

Received: January 16, 2013
Published online: April 5, 2013

[1] U. Bach, D. Lupo, P. Comte, J. E. Moser, F. Weissörtel, J. Salbeck, H. Spreitzer, M. Grätzel, *Nature* **1998**, *395*, 583.
[2] C.-Y. Hsu, Y.-C. Chen, R. Y.-Y. Lin, K.-C. Ho, J. T. Lin, *Phys. Chem. Chem. Phys.* **2012**, *14*, 14099.
[3] B. E. Hardin, H. J. Snaith, M. D. McGehee, *Nat. Photon.* **2012**, *6*, 162.
[4] C. Xu, J. Wu, U. V Desai, D. Gao, *Nano Lett.* **2012**, *12*, 2420.
[5] P. Chen, J. H. Yum, F. De Angelis, E. Mosconi, S. Fantacci, S.-J. Moon, R. H. Baker, J. Ko, M. K. Nazeeruddin, M. Grätzel, *Nano Lett.* **2009**, *9*, 2487.
[6] H. J. Snaith, *Adv. Funct. Mater.* **2010**, *20*, 13.
[7] A. Dualeh, R. Humphry-Baker, J. H. Delcamp, M. K. Nazeeruddin, M. Grätzel, *Adv. Energy Mater.* **2012**, DOI: 10.1002/aenm.201200701.
[8] A. Yella, H.-W. Lee, H. N. Tsao, C. Yi, A. K. Chandiran, M. K. Nazeeruddin, E. W.-G. Diau, C.-Y. Yeh, S. M. Zakeeruddin, M. Grätzel, *Science* **2011**, *334*, 629.
[9] A. Hagfeldt, G. Boschloo, L. Sun, L. Kloo, H. Pettersson, *Chem. Rev.* **2010**, *110*, 6595.
[10] J. Burschka, A. Dualeh, F. Kessler, E. Baranoff, N.-L. Cevey-Ha, C. Yi, M. K. Nazeeruddin, M. Grätzel, *J. Am. Chem. Soc.* **2011**, *133*, 18042.
[11] N. Cai, S.-J. Moon, L. Cevey-Ha, T. Moehl, R. Humphry-Baker, P. Wang, S. M. Zakeeruddin, M. Grätzel, *Nano Lett.* **2011**, *11*, 1452.
[12] S. Wenger, M. Schmid, G. Rothenberger, A. Gentsch, M. Grätzel, J. O. Schumacher, *J. Phys. Chem. C* **2011**, *115*, 10218.
[13] A. Dualeh, F. De Angelis, S. Fantacci, T. Moehl, C. Yi, F. Kessler, E. Baranoff, M. K. Nazeeruddin, M. Grätzel, *J. Phys. Chem. C* **2012**, *116*, 1572.
[14] H. J. Snaith, R. Humphry-Baker, P. Chen, I. Cesar, S. M. Zakeeruddin, M. Grätzel, *Nanotechnology* **2008**, *19*, 424003.
[15] L. Schmidt-Mende, M. Grätzel, *Thin Solid Films* **2006**, *500*, 296.
[16] M. Yanagida, N. Onozawa-Komatsuzaki, M. Kurashige, K. Sayama, H. Sugihara, *Sol. Energy Mater. Sol. Cells* **2010**, *94*, 297.
[17] G. F. Burkhard, E. T. Hoke, S. R. Scully, M. D. McGehee, *Nano Lett.* **2009**, *9*, 4037.
[18] G. F. Burkhard, E. T. Hoke, M. D. McGehee, *Adv. Mater.* **2010**, *22*, 3293.
[19] D. M. Huang, H. J. Snaith, M. Grätzel, K. Meerholz, A. J. Moulé, *J. Appl. Phys.* **2009**, *106*, 073112.
[20] A. J. Moulé, H. J. Snaith, M. Kaiser, H. Klesper, D. M. Huang, M. Grätzel, K. Meerholz, *J. Appl. Phys.* **2009**, *106*, 073111.
[21] M. M. Lee, J. Teuscher, T. Miyasaka, T. N. Murakami, H. J. Snaith, *Science* **2012**, *338*, 643.
[22] H.-S. Kim, C.-R. Lee, J.-H. Im, K.-B. Lee, T. Moehl, A. Marchioro, S.-J. Moon, R. Humphry-Baker, J.-H. Yum, J. E. Moser, M. Grätzel, N.-G. Park, *Sci. Rep.* **2012**, *2*, 1.
[23] I. Chung, B. Lee, J. He, R. P. H. Chang, M. G. Kanatzidis, *Nature* **2012**, *485*, 486.
[24] S.-J. Moon, Y. Itzhaik, J.-H. Yum, S. M. Zakeeruddin, G. Hodes, M. Grätzel, *J. Phys. Chem. Lett.* **2010**, *1*, 1524.
[25] H. Sakamoto, S. Igarashi, M. Uchida, K. Niume, M. Nagai, *Org. Electron.* **2012**, *13*, 514.
[26] J.-J. Cid, J.-H. Yum, S.-R. Jang, M. K. Nazeeruddin, E. Martínez-Ferrero, E. Palomares, J. Ko, M. Grätzel, T. Torres, *Angew. Chem. Int. Edit.* **2007**, *46*, 8358.
[27] L. Schmidt-Mende, S. M. Zakeeruddin, M. Grätzel, *Appl. Phys. Lett.* **2005**, *86*, 013504.
[28] L. A. A. Pettersson, L. S. Roman, O. Inganäs, *J. Appl. Phys.* **1999**, *86*, 487.
[29] U. B. Cappel, T. Daeneke, U. Bach, *Nano Lett.* **2012**, *12*, 4925.
[30] S. Fantacci, F. De Angelis, M. K. Nazeeruddin, M. Grätzel, *J. Phys. Chem. C* **2011**, *115*, 23126.
[31] A. Abate, T. Leijtens, S. Pathak, J. Teuscher, R. Avolio, M. E. Errico, J. Kirkpatrik, J. M. Ball, P. Docampo, I. McPherson, H. J. Snaith, *Phys. Chem. Chem. Phys.* **2013**, *15*, 2572.
[32] J. Melas-Kyriazi, I.-K. Ding, A. Marchioro, A. Punzi, B. E. Hardin, G. F. Burkhard, N. Tétreault, M. Grätzel, J.-E. Moser, M. D. McGehee, *Adv. Energy Mater.* **2011**, *1*, 407.
[33] P. Docampo, A. Hey, S. Guldin, R. Gunning, U. Steiner, H. J. Snaith, *Adv. Funct. Mater.* **2012**, *22*, 5010.
[34] I.-K. Ding, N. Tétreault, J. Brillet, B. E. Hardin, E. H. Smith, S. J. Rosenthal, F. Sauvage, M. Grätzel, M. D. McGehee, *Adv. Funct. Mater.* **2009**, *19*, 2431.
[35] H. Snaith, L. Schmidt-Mende, M. Grätzel, M. Chiesa, *Phys. Rev. B* **2006**, *74*, 045306.
[36] S. E. Koops, B. C. O'Regan, P. R. F. Barnes, J. R. Durrant, *J. Am. Chem. Soc.* **2009**, *131*, 4808.
[37] E. M. Barea, J. Ortiz, F. J. Payá, F. Fernández-Lázaro, F. Fabregat-Santiago, A. Sastre-Santos, J. Bisquert, *Energ. Environ. Sci.* **2010**, *3*, 1985.
[38] J.-H. Yum, S.-R. Jang, R. Humphry-Baker, M. Grätzel, J.-J. Cid, T. Torres, M. K. Nazeeruddin, *Langmuir* **2008**, *24*, 5636.
[39] M.-E. Ragoussi, J.-J. Cid, J.-H. Yum, G. de la Torre, D. Di Censo, M. Grätzel, M. K. Nazeeruddin, T. Torres, *Angew. Chem. Int. Edit.* **2012**, *51*, 4375.

© 2013 WILEY-VCH Verlag GmbH & Co. KGaA, Weinheim

[40] T. Marinado, M. Hahlin, X. Jiang, M. Quintana, E. M. J. Johansson, E. Gabrielsson, S. Plogmaker, D. P. Hagberg, G. Boschloo, S. M. Zakeeruddin, M. Grätzel, H. Siegbahn, L. Sun, A. Hagfeldt, H. Rensmo, *J. Phys. Chem. C* **2010**, *114*, 11903.
[41] J. Lim, Y. S. Kwon, T. Park, *Chem. Commun.* **2011**, *47*, 4147.
[42] M. Wang, C. Grätzel, S.-J. Moon, R. Humphry-Baker, N. Rossier-Iten, S. M. Zakeeruddin, M. Grätzel, *Adv. Funct. Mater.* **2009**, *19*, 2163.
[43] Y. S. Kwon, I. Y. Song, J. Lim, S.-H. Park, A. Siva, Y.-C. Park, H. M. Jang, T. Park, *RSC Adv.* **2012**, *2*, 3467.
[44] J. Krüger, U. Bach, M. Grätzel, *Adv. Mater.* **2000**, *12*, 447.
[45] N. R. Neale, N. Kopidakis, J. van de Lagemaat, M. Grätzel, A. J. Frank, *J. Phys. Chem. B* **2005**, *109*, 23183.
[46] I.-K. Ding, J. Zhu, W. Cai, S.-J. Moon, N. Cai, P. Wang, S. M. Zakeeruddin, M. Grätzel, M. L. Brongersma, Y. Cui, M. D. McGehee, *Adv. Energy Mater.* **2011**, *1*, 52.

© 2013 WILEY-VCH Verlag GmbH & Co. KGaA, Weinheim